

Article

Non-Line-of-Sight Atmospheric Optical Communication in the Visible Wavelength Range between UAV and the Ground Surface

Mikhail V. Tarasenkov *, Egor S. Poznakharev and Andrey V. Fedosov

V.E. Zuev Institute of Atmospheric Optics SB RAS, 1, Academician Zuev Square, 634055 Tomsk, Russia; 724_pes1992@iao.ru (E.S.P.); fean@iao.ru (A.V.F.)

* Correspondence: tmv@iao.ru

Abstract: An opto-electronic system for non-line-of-sight (NLOS) communication using scattered laser radiation for unmanned aerial vehicle (UAV)–ground and ground–UAV schemes at a wavelength of $\lambda = 450$ nm and a ground–UAV scheme at a wavelength of $\lambda = 510$ nm are described. The symbol error rate (SER) and its standard deviation were analyzed for different schemes of the communication channel. The transceiver system included a laser source with a power supply, a modulator, a lens refractor, a bandpass filter, a photomultiplier tube (PMT), a demodulator, and a receiving computer. The experimental data obtained at nighttime showed that the NLOS atmospheric optical communication at a wavelength of $\lambda = 450$ nm was feasible for the UAV–ground scheme at a baseline distance of up to 150 m for a UAV with a transmitter at a height of 10 m and at a baseline distance of up to 125 m for a UAV at a height of 20 m. For the ground–UAV scheme, stable communication was observed at baseline distances of up to 50 m for a UAV with a receiver at a height up to 30 m. The NLOS atmospheric optical communication at a wavelength of 510 nm was obtained for the ground–UAV scheme at baseline distances of up to 100 m for a UAV with a receiver at a height up to 45 m, as well as at baseline distances of up to 385 m for UAV flying at a height up to 20 m.

Keywords: NLOS optical communication; visible range; unmanned aerial vehicle; scattered laser radiation; field experiments



Citation: Tarasenkov, M.V.; Poznakharev, E.S.; Fedosov, A.V. Non-Line-of-Sight Atmospheric Optical Communication in the Visible Wavelength Range between UAV and the Ground Surface. *Atmosphere* **2024**, *15*, 21. [10.3390/atmos15010021](https://doi.org/10.3390/atmos15010021)

Academic Editors: Konrad Bärffuss and Barbara Harm-Altstädter

Received: 15 November 2023

Revised: 14 December 2023

Accepted: 20 December 2023

Published: 24 December 2023



Copyright: © 2023 by the authors. Licensee MDPI, Basel, Switzerland. This article is an open access article distributed under the terms and conditions of the Creative Commons Attribution (CC BY) license (<https://creativecommons.org/licenses/by/4.0/>).

1. Introduction

Owing to the advent of smart and remote monitoring technologies, the last decade has been characterized by a drastic development of unmanned devices. One of the fastest-growing research fields is the technology associated with unmanned aerial vehicles (UAVs). This opens up opportunities for UAV use in fields such as video surveillance and remote sensing of the Earth's surface, the delivery of small-sized cargo, etc. A new direction in the development of the UAV technologies is wireless optical communication, which is resistant to radio frequency interference, characterized by high data rates and not requiring the licensing of the frequency range.

There are several directions for the development of wireless optical communication technologies with UAVs. The reviews [1,2] noted that UAVs can be used for communication with satellites, other UAVs, underwater and over-water objects, and ground objects in the terahertz and optical ranges. Within the framework of the analysis performed, the following fields in the study of optical communication channels using UAVs can be identified:

- (1) Line-of-sight (LOS) wireless communication in the radio and optical ranges between a ground object and a satellite [3–5];
- (2) LOS hybrid wireless communication in the radio and optical ranges between land and water surface objects [6–9];
- (3) LOS wireless optical communication [10–15];
- (4) Combined LOS-NLOS wireless optical communication [16–18];

- (5) NLOS wireless optical communication in the atmosphere in the ultraviolet (UV) range [19–21].

NLOS atmospheric optical communication with UAVs has the following applications: (1) multicast communication; (2) communication in situations when the direct visibility of the source is screened by an obstacle (in urban areas, forests, or mountains); (3) unauthorized access to a communication channel in direct visibility; (4) the formation and control of UAV groups (swarms).

The studies of NLOS optical communication with UAVs are based on the results obtained for NLOS communications between ground-based objects that began with papers such as [22,23]. At the beginning of the 21st Century, the development of small-sized laser sources and highly sensitive optical receivers has caused a sharp growth in the interest of specialists in studying the feasibility of NLOS wireless optical communications [24]. We consider the papers [25–31] to be the most-important from the viewpoint of developing the theory and experimental studies of NLOS communication feasibility. As a part of the work on terrestrial NLOS communications in the open atmosphere, the following most-important results were obtained: (1) methods for statistical simulation of the impulse response of a communication channel have been developed; (2) analytical equations have been proposed for the single scattered part of the impulse response; (3) interpolation equations have been proposed for the impulse response and the path loss; (4) the received signal duration as a function of a wide range of optical–geometric conditions has been assessed; (5) equations have been proposed for calculating the bit error rate (BER), symbol error rate (SER), and package error rate (PER) for a wide range of modulation methods; (6) the dependence of the BER, signal-to-noise ratio (SNR), and maximum data rate on a wide range of optical and geometric conditions and source parameters for the main information encoding methods has been assessed; (7) the effect of turbulence on the path loss under day and night conditions has been evaluated.

The earlier studies of NLOS wireless atmospheric communications with UAVs have yielded the following results. A Monte Carlo model of the communication channel for the UAV–ground and ground–UAV schemes was developed in [16]. Favorable and unfavorable geometric conditions for organizing UV communication, whose coverage area may contain a bugging device, were considered, and the sensitivity of a UV communication channel to various geometric conditions was analyzed. The communication channel’s characteristics were experimentally assessed, and the possibilities of identifying and locating multibeam sources in both LOS and NLOS communications between two hexacopters in an urban environment were considered in [17]. The equation for calculating the communication range for LOS and NLOS channels was analyzed based on the UV communication channel model, and the 3D algorithm for UAV localizing in space was proposed [18]. The effect of interfering sources on the NLOS UV communication system’s performance was numerically assessed using the BER for UV uplink communications between ground-based sources and UAVs in the atmosphere [19]. A model of the NLOS UV uplink with scattering between ground-based sources and UAVs that are placed in series was considered in [20]. This model was used to evaluate the performance of a communication system as a function of parameters such as the divergence of a source beam and the receiver’s field of view and to determine the maximum UAV coverage to maintain a certain BER value. An algorithm for controlling a UAV formation with one or several main aircraft via the NLOS wireless optical communication channel for autonomous restoration of the UAV formation, preventing collisions between the UAVs, and the flocking of the UAV formation was developed in [21].

It was noted in the papers [16–21] that NLOS wireless optical communication at radiation wavelengths of 240–270 nm is possible at a maximum range of 1.2 km. The analysis of the available publications showed that, currently, most of the papers on NLOS wireless optical communication with UAVs deal with theoretical studies of the communication channel and primarily consider the wavelength range of 240–270 nm. However, experimental studies of this type of communication under field conditions are currently lacking.

Our earlier experimental studies [32–34] dealing with terrestrial NLOS communication yielded the following results. It was shown that a stable terrestrial NLOS wireless optical communication can be organized at baseline distances up to 70 km. In addition, the possibility of implementing stable NLOS optical communication in the UV wavelength range at a baseline distance of up to 1.3 km in day and night was demonstrated.

This paper describes an experimental model for NLOS atmospheric optical communications by the UAV–ground and ground–UAV schemes in the visible wavelength range. The visible range was chosen since it is fully safe for humans and there are small-sized and sufficiently powerful laser radiation sources in this wavelength range. The aim of the study was to assess the feasibility of NLOS wireless optical communication under field conditions in a range up to 400 m and a UAV height up to 45 m in the dark.

2. Investigation Methodology

Optical communication channels were studied with a transceiver system, whose block diagram is shown in (Figure 1). The operating principle of the communication system was as follows. A modulator with the successive generation of symbols from 0 to 255 in the binary system in continuous mode generates electrical pulses (Figure 2a) at a laser source using the differential pulse-interval modulation (DPIM). The laser power supply is connected to batteries or a 220 V network, and the laser source generates radiation and sends information laser pulses into the atmospheric communication channel. Laser radiation scattered by molecules or aerosol is detected by the receiving system within the field of view of the lens refractor through a bandpass filter on the input window of the photomultiplier tube (PMT). Electrical signals from the PMT (Figure 2b) are recognized by the demodulator and recorded in numerical form on a laptop to estimate the SER and its standard deviation. The SER and the standard deviations are estimated for 1000 recorded symbols in one package. The duration of the communication session is 1 min 50 s with the recording of 10 packages.

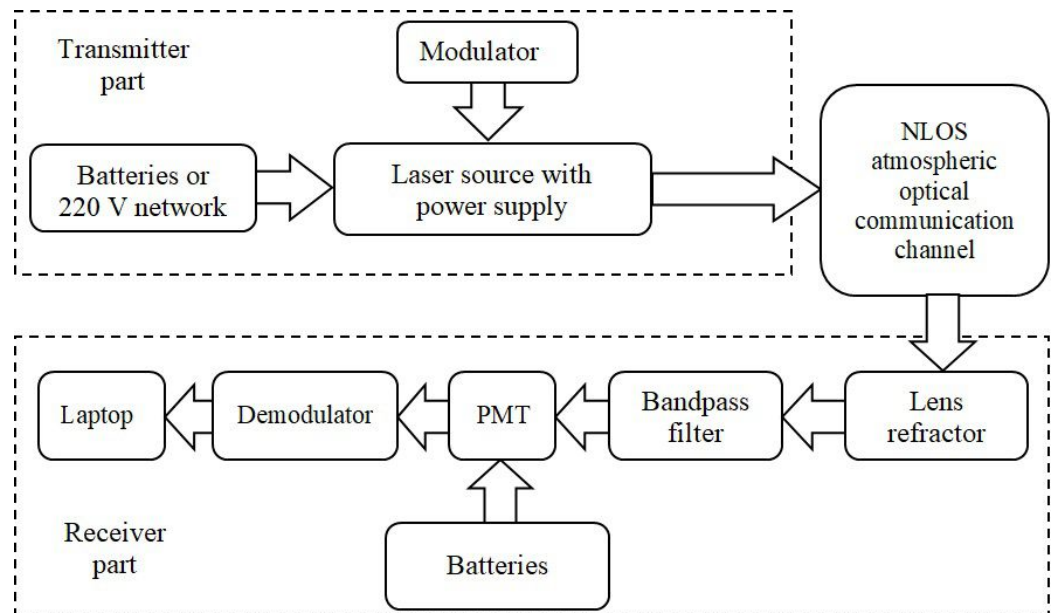


Figure 1. Block diagram of the NLOS wireless optical communication system used.

To assess the communication quality, we used the values of the SER in one package of symbols P_e , the average SER for communication session \bar{P}_e , and the standard deviations $\bar{\sigma}$, which were determined as [32]:

$$P_{e,j} = \frac{\sum_{i=1}^n x_i}{n} \quad (1)$$

$$\bar{P}_e = \frac{1}{M} \sum_{j=1}^M P_{e,j} \tag{2}$$

$$\bar{\sigma} = \sqrt{\frac{1}{n} \sum_{i=1}^n (x_i - P_e)^2} \tag{3}$$

where x_i are the error symbols; n is the total number of symbols in a single package ($n = 1000$); M is the number of packages in a single communication session ($M = 10$).

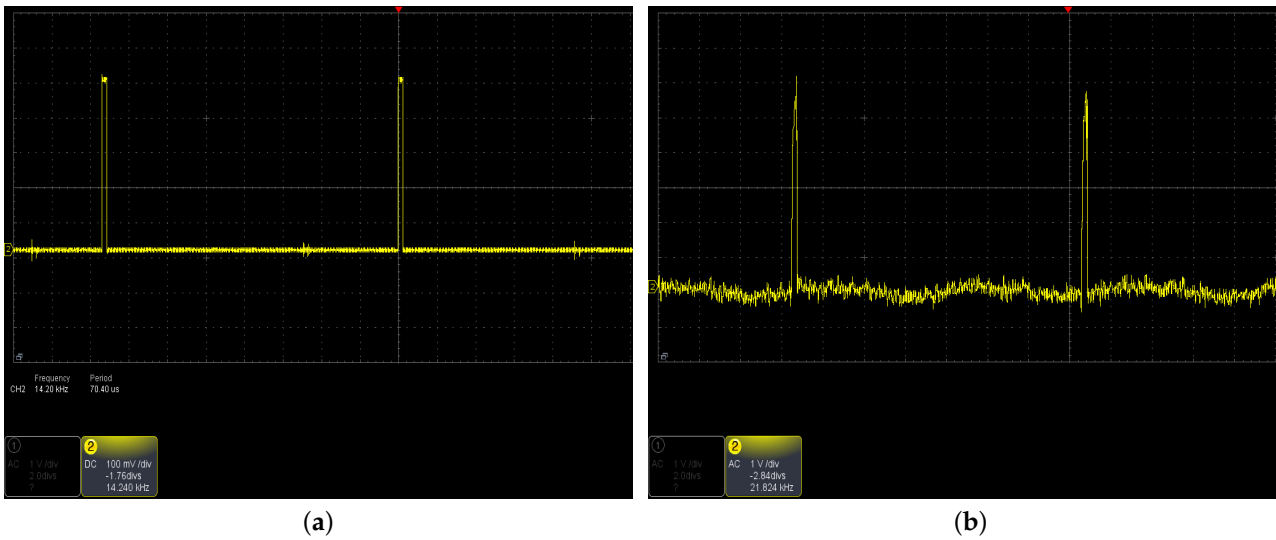


Figure 2. Examples of transmitted and received signals: (a) transmitted pulses; (b) received pulses.

The communication channel was tested for symbol packages as illustrated in Figure 3. When symbols are transmitted without error, the image of the test object is similar to that shown in Figure 3a. The presence of such a test object on the laptop monitor indicates that there is no influence of external interfering sources or the atmospheric environment on the communication channel. Figure 3b exemplifies a significant impact of interfering sources on the transmitted signal. In the experiments, $\bar{P}_e = 0.1$ was considered as a limit, at which the communications is stable.

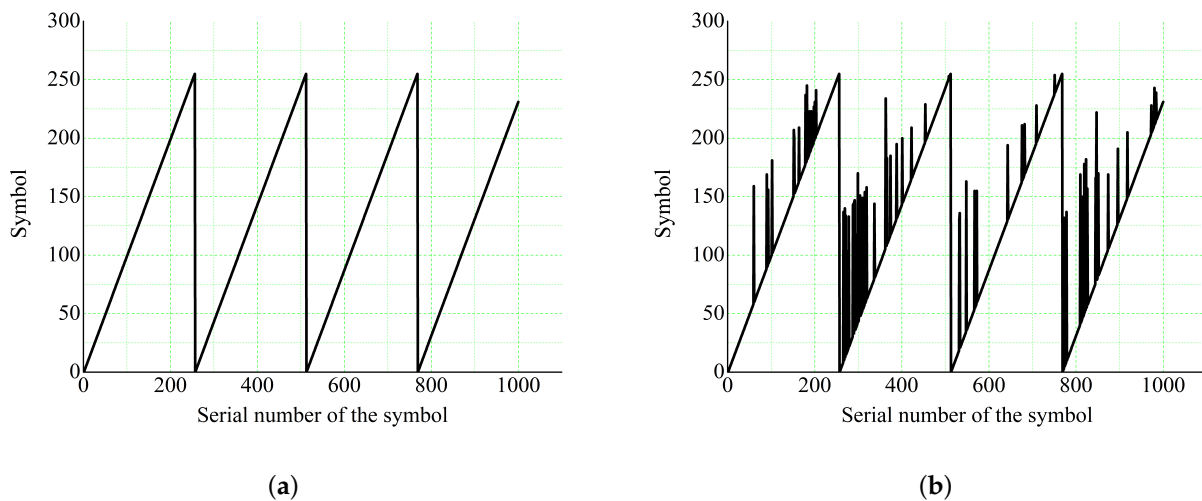


Figure 3. Graphical test object received through an atmospheric channel with scattering: (a) undistorted test object; (b) distorted test object.

3. Experimental Setup

Three series of field experiments were conducted: (1) NLOS optical communication at a wavelength of $\lambda = 450$ nm with a UAV-borne source and a ground-based receiving system; (2) NLOS optical communication at a wavelength of $\lambda = 450$ nm with a ground-based source and a UAV-borne receiving system; (3) NLOS optical communication at a wavelength $\lambda = 510$ nm with a ground-based source and a UAV-borne receiving system. The NLOS wireless optical communication systems with the UAV were constructed according to a one-way communication (simplex) scheme using transceiver systems with the characteristics shown in Table 1. In different experimental series, the source (or receiving system) was installed onboard the DJI Agras T10 UAV (SZ DJI Technology Co., Shenzhen, China) with a payload of up to 10 kg and a flight duration up to 15 min. The use of this type of UAV allowed us to avoid problems with balancing the instruments installed on the UAV and payload limitations. Figure 4a shows how the transmitting system was installed onboard the UAV. A similar transmitting system was used in the second series of experiments. In experimental series 1 and 2, the transmitting systems consisted of an NEJE N30820 laser unit (Shenzhen Zhixinjie Technology Co., Shenzhen, China) generating radiation at a wavelength of $\lambda = 450$ nm, a power driver, batteries, a modulator, a display, and buttons for adjusting the data transmission characteristics. The choice of a laser source at this wavelength was due to its small size, relatively low cost, and the capability to convert continuous-wave radiation into pulses with a pulse-generation frequency higher than 10 kHz and a signal duration of 2 μ s. In experimental series 3, we used a transmitting system (Figure 4b) consisting of a copper bromide vapor laser source generating radiation at a wavelength of 510 nm, a modulator, and a mirror directing the radiation to the desired spatial region. The choice of the laser at this wavelength was due to its capability of generating radiation with high energy per pulse. In this study, we dealt with communication channels in the visible wavelength range since they are safe for humans, unlike sources in the UV range.

The receiving system in experimental series 1 and 2 (Figure 4c) comprised a lens refractor, a semrock brightline fluorescence bandpass filter 442/42 (IDEX Health and Science, Kawaguchi, Japan), a UFK-4G-2 PMT (KATOD, Moscow, Russian Federation), a signal decoding device, batteries, and a laptop. In experimental series 3, we used the semrock brightline fluorescence filter FF03-510/20-25 (IDEX Health and Science, Kawaguchi, Japan) as a bandpass filter. The receiving system in series 2 and 3 (Figure 4d) was mounted on the UAV, while in series 1, it was mounted on a tripod for stable placement on the ground.

Table 1. Parameters of the transceiver system and its location during field experiments.

Parameter	Experimental Series 1	Experimental Series 2	Experimental Series 3
Wavelength λ , nm	450	450	510
Energy per pulse Q , μ J	12	12	28
Pulse duration τ	2 μ s	2 μ s	30 ns
Pulse repetition frequency ν , kHz	14	14	14
Source zenith angle θ_s	88°	45°	45°
Horizontal divergence angle α_H	0.37°	0.37°	0.0034°
Vertical divergence angle α_V	0.08°	0.08°	0.0034°
Detector zenith angle θ_d	45°	88°	88°
Field-of-view angle ψ	20°	2°	2°
Source height above the ground h_s , m	10, 20, 30	0.5	0.5

Table 1. Cont.

Parameter	Experimental Series 1	Experimental Series 2	Experimental Series 3
Receiver height above the ground h_r , m	0.5	10, 20, 30	10, 20, 30, 40, 45
Baseline distance Y_N , m	25, 50, 75, 100, 125, 150	25, 50	50, 75, 100, 150, 200, 385

The experiments were carried out on 8 September 2022 (series 1), 27 July 2023 (series 2), and 26 August 2023 (series 3) at the IAO SB RAS test site in the dark according to a coplanar communication scheme. The experiments on 8 September 2022 were carried out under a clear sky, an air temperature of +6 °C, and a wind speed of 2 m/s. On 27 July 2023, the experiments were conducted under a cloudy sky, an air temperature of +19 °C, and a wind speed of 1 m/s. On 26 August 2023, the air temperature during the experiment was +13 °C, the wind speed was 1 m/s, and the sky was clear.



(a)



(b)



(c)



(d)

Figure 4. NLOS wireless optical communication transceiver systems for the UAV–ground and ground–UAV schemes: (a) transmitting system in experimental series 1; (b) transmitting system in experimental series 3; (c) receiving system in experimental series 1; (d) receiving system in experimental series 2 and 3.

The field studies were carried out in the following way. In experimental series 1 (Figure 5a), the source S was set on the UAV and oriented at a zenith angle of 88° in accordance with the height difference at the test site. The UAV was raised to a height of 10 to 30 m depending on the experiment. The receiving system was located on the ground at a baseline distance of 25 to 150 m from the UAV. The baseline distance is the separation between the projections of the transmitting and receiving systems on the ground. The optical axis of the receiving system was oriented at a zenith angle of 45° in the direction of the source. In experimental series 2 (Figure 5b), a transmitting system similar to that in series 1 was set on the ground. The optical axis of the source was oriented at a zenith angle of 45° . The receiving system was set on the UAV. The optical axis of the receiving system was oriented at a zenith angle of 88° from the vertical. The UAV with the receiving system was raised to a height of 10 to 30 m, depending on the experiment, and placed at a baseline distance of 25 to 50 m. In experimental series 3 (Figure 5c), in contrast to series 1 and 2, the ground-based transmitting system at a wavelength of $\lambda = 510 \text{ nm}$ was used. The receiving system was set on the UAV and raised to a height of 10 to 45 m, depending on the experiment. The baseline distance in series 3 varied from 50 to 385 m.

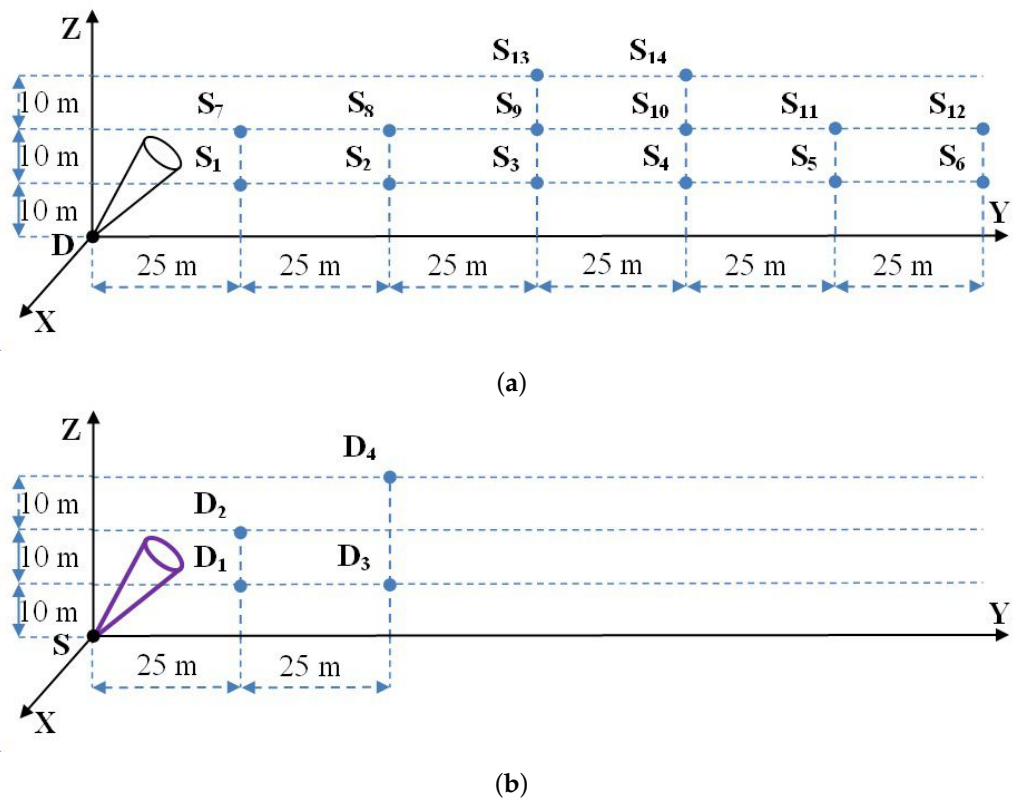


Figure 5. Cont.

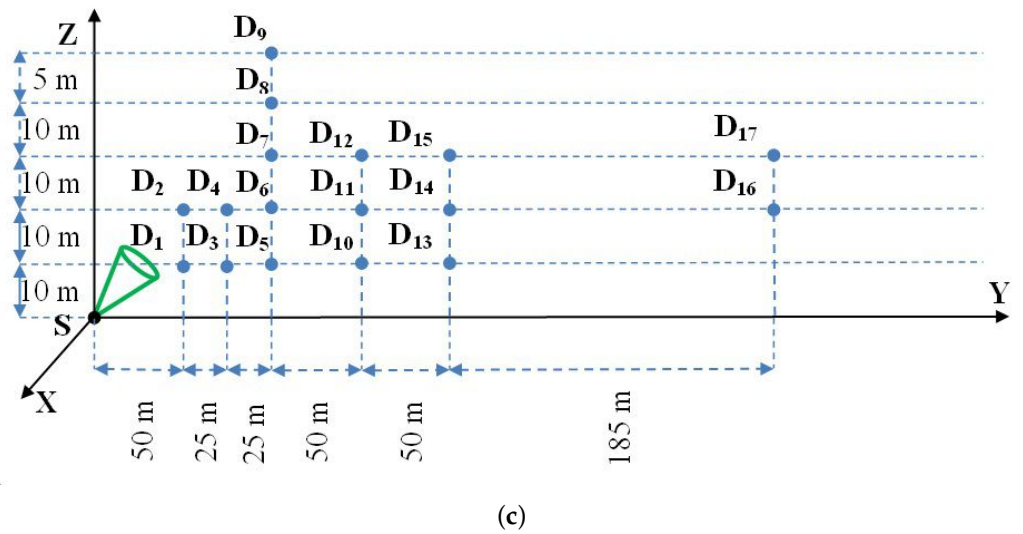


Figure 5. Schemes of field experiments to assess the capabilities of NLOS wireless atmospheric optical communications: (a) experimental series 1 ($\lambda = 450$ nm, the transmitting system on the UAV and the receiving system on the ground); (b) experimental series 2 ($\lambda = 450$ nm, the transmitting system on the ground and the receiving system on the UAV); (c) experimental series 3 ($\lambda = 510$ nm, the transmitting system on the ground and the receiving system on the UAV).

4. Result and Discussions

The SERs and their standard deviations obtained by Equations (1)–(3) for the conducted experiments are given in Tables 2–4. Figure 6 exemplifies the measured SERs and their standard deviations for a communication session. The analysis of the results obtained in experimental series 1 showed that the SER at the baseline distance $Y_N = 25$ m was higher than at $Y_N = 50$ m, likely because the scattering volume was smaller for the smaller baseline distance. The maximum baseline distance of stable communication at $h_s = 10$ m was $Y_N = 150$ m with a SER of $\bar{P}_e \leq 0.22$. At $h_s = 20$ m, the maximum range of stable communication was $Y_N = 125$ m with a SER of $\bar{P}_e \leq 0.23$. At $h_s = 30$ m in experimental series 1, we failed to establish a stable communication. In experimental series 2, we managed to establish a stable communication up to a height of $h_r = 30$ m and a baseline distance of $Y_N = 50$ m. For a longer Y_N , the communication could not be established. The maximum communication range in experimental series 2 was smaller than that in series 1, because the receiving system set on the UAV employed a telescope with a smaller aperture and field-of-view angle. In experimental series 3, the communication range was significantly longer than in experimental series 2 due to the use of a laser with higher pulse energy in the transmitting system. The conducted experiments showed that, for baseline distances up to 100 m, a stable communication was feasible for heights up to $h_r = 45$ m. At baseline distances of $150 \leq Y_N \leq 385$ m, a stable communication was observed at $h_r \leq 20$ m. At heights of $h_r = 30$ m and $Y_N \geq 150$ m, the communication was unstable. For the transceiver system used in experimental series 3, the maximum communication range was $Y_N \sim 385$ m at $h_r \leq 20$ m with $\bar{P}_e \leq 0.1$.

Table 2. SERs (\bar{P}_e) and their standard deviations ($\bar{\sigma}$) for series 1 of field experiments.

$Y_N, \text{ m}$	$h_s, \text{ m}$					
	10		20		30	
	\bar{P}_e	$\bar{\sigma}$	\bar{P}_e	$\bar{\sigma}$	\bar{P}_e	$\bar{\sigma}$
25	0.0002	0.0011	0.0281	0.0313	-	-
50	0.0001	0.0006	0.0045	0.0134	-	-

Table 2. Cont.

$Y_N, \text{ m}$	$h_s, \text{ m}$					
	10		20		30	
	\bar{P}_e	$\bar{\sigma}$	\bar{P}_e	$\bar{\sigma}$	\bar{P}_e	$\bar{\sigma}$
75	0.0002	0.0011	0.0064	0.0150	0.9517	0.0846
100	0.0008	0.0035	0.0206	0.0292	0.9038	0.1316
125	0.0268	0.0589	0.2315	0.2485	-	-
150	0.2188	0.2739	0.2994	0.1849	-	-

Table 3. SERs (\bar{P}_e) and their standard deviations ($\bar{\sigma}$) for series 2 of field experiments.

$Y_N, \text{ m}$	$h_r, \text{ m}$					
	10		20		30	
	\bar{P}_e	$\bar{\sigma}$	\bar{P}_e	$\bar{\sigma}$	\bar{P}_e	$\bar{\sigma}$
25	0	0	0.0002	0.0009	-	-
50	0.0200	0.0461	-	-	0.0808	0.0654

Table 4. SERs (\bar{P}_e) and their standard deviations ($\bar{\sigma}$) for series 3 of field experiments.

$Y_N, \text{ m}$	$h_r, \text{ m}$	\bar{P}_e	$\bar{\sigma}$
50	10	0	0
	20	0	0
75	10	0	0
	20	0.002	0.006
100	10	0	0
	20	0	0
	30	0	0
	40	0	0
	45	0	0
150	10	0	0
	20	0.021	0.028
	30	0.517	0.129
200	10	0.001	0.002
	20	0.002	0.007
	30	0.444	0.092
385	20	0.099	0.084
	30	0.694	0.179

As the baseline distance increases, an increase in the SER should be observed at a sufficient distance from the source. However, a non-monotonic behavior was observed sometimes, for example, in the following situations: series 1 for $h_s = 30 \text{ m}$ and $Y_N = 75$ and 100 m and series 3 for $h_r = 20 \text{ m}$ and $Y_N = 150$ and 200 m . In the first case, the SER was close to 1. This means that nearly all symbols were received with errors, and in addition, the standard deviation was very large. In this case, the non-monotonic behavior of the SER with an increase of Y_N was caused by random errors in the communication channel.

In the second case, the non-monotonic behavior can be explained by slight turns of the UAV under the effect of the wind. Therefore, an increase/decrease in the SER can be observed at a fairly large distance depending on the wind.

For some packages in a communication session, rather wide SER variations were observed (see, for example, Figure 6c). These variations were caused by the fact that the optical axis of the equipment installed on the UAV turned under the effect of the wind. The wind effect increased with an increase of the baseline distance. To analyze this factor for several situations, the experiments were conducted several times. The comparison showed that the limiting baseline distances of stable communication varied insignificantly (by a few meters) from one experiment to another.

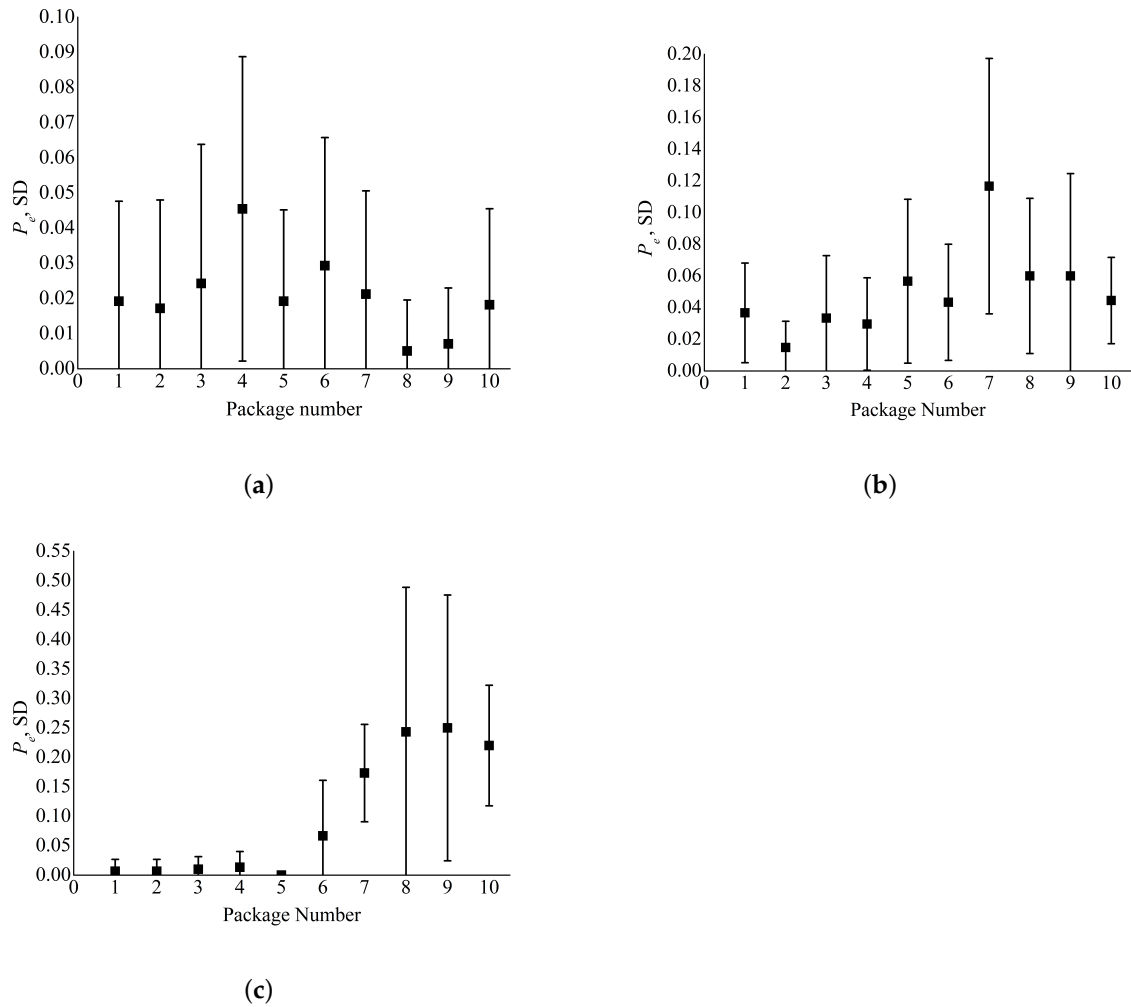


Figure 6. Examples of the obtained SERs and their standard deviations (SDs) for a communication session: (a) experimental series 1, $Y_N = 100$ m, $h_s = 20$ m; (b) experimental series 2, $Y_N = 50$ m, $h_r = 30$ m; (c) experimental series 3, $Y_N = 150$ m, $h_r = 20$ m.

In the experiments conducted, there were no obstacles between the transmitting and receiving systems, because the testing ground was flat (without trees and buildings). The considered communication schemes exclude the possibility of line-of-sight receiving. In addition, using the earlier-developed algorithm [35], we calculated the impulse response of the communication channel for situations similar to those in the experiments and estimated the influence of radiation, which could be blocked by an obstacle. The calculations were performed for the following optical and geometric conditions: $\lambda = 450$ and 510 nm; MODTRAN midlatitude summer atmospheric model [36]; extinction coefficients of the surface atmospheric layer (sum of the molecular and aerosol extinction)

$\sigma_{e,450} = 9.36 \times 10^{-2} \text{ km}^{-1}$, $\sigma_{e,510} = 7.63 \times 10^{-2} \text{ km}^{-1}$; scattering coefficients of the surface atmospheric layer $\sigma_{s,450} = 8.99 \times 10^{-2} \text{ km}^{-1}$, $\sigma_{s,510} = 7.24 \times 10^{-2} \text{ km}^{-1}$. The baseline distances, UAV heights, receiver's aperture area, divergence angles of the radiation source, receiver's field of view, and zenith angles of the optical axes of the source and the receiver were set the same as in the field experiments. The estimates (Table 5) showed that the contribution of the single scattered radiation to the useful signal in the considered situations was $\delta_1 \geq 84.2\%$, while the fraction of the useful signal, which came through the space within the divergence angle of the source radiation and the field of view of the receiving system, was $\delta \geq 92\%$. Thus, if an obstacle does not block the field of view of the receiving system and the area of the divergence of the source radiation, then it cannot reduce the useful signal by a value greater than 8% under the conditions of our experiments. For this reason, the experiments conducted provided a rather good idea about the capabilities of similar communication systems. In our future studies, we plan to consider the capabilities of implementing NLOS optical communication schemes with an obstacle not violating legal restrictions on the use of UAVs.

Table 5. Minimal $\delta_{1,min}$ and maximal $\delta_{1,max}$ fractions of the useful signal single scattered by the atmosphere, as well as the minimal δ_{min} and maximal δ_{max} fractions of radiation coming to the receiving system from the area of divergence of the source radiation and the field of view of the receiving system.

Experimental Series	$\delta_{1,min}$	$\delta_{1,max}$	δ_{min}	δ_{max}
1	0.842	0.913	0.920	0.962
2	0.945	0.996	0.963	0.997
3	0.865	1.000	0.927	1.000

The transceiving system used in our experiments employed DPIM. In the previous papers dealing with NLOS optical communication, modulations such as on-off-keying (OOK), pulse position modulation (PPM), dual-head pulse interval modulation (DH-PIM), frequency-shift keying (FSK), spectral amplitude coding (SAC), and others were used. The choice of the DPIM modulation is quite justified, since it was shown, for example, in [29] that this type of communication modulation potentially allows more symbols to be transmitted per unit time than, for example, OOK.

The obtained results do not contradict the results reported in the works [19,20,37]. It was estimated in the paper [20] that the NLOS optical communication with a BER $\leq 10^{-6}$ at a wavelength of 254 nm is possible at a UAV height of 50 m and a baseline distance of 25.7 m. In the work [19], it was shown that the NLOS optical communication at a wavelength of 265 nm with a BER $\leq 10^{-6}$ by the same scheme as in the work [20] is feasible at a UAV height of 100 m and a baseline distance of 75 m. For the ground-based communication scheme in the UV wavelength range, it was shown experimentally in [37] that the NLOS optical communication is implementable at a baseline distance of 164 m.

5. Conclusions

The following most-important results were obtained:

- (1) With the developed transceiver system at a wavelength of $\lambda = 450 \text{ nm}$ for the UAV-ground scheme, the maximum baseline distance of stable communication at a UAV height of $h_s = 10 \text{ m}$ was $Y_N = 150 \text{ m}$ with an SER of $\bar{P}_e \leq 0.22$. At $h_s = 20 \text{ m}$, the maximum range of stable communication was $Y_N = 125 \text{ m}$ with an SER of $\bar{P}_e \leq 0.23$. At a height of $h_s = 30 \text{ m}$, we failed to establish a stable communication in experimental series 1.
- (2) The use of the developed transceiver system at a wavelength of $\lambda = 450 \text{ nm}$ allowed a stable communication by the ground-UAV scheme to be organized only for a baseline distance of $Y_N = 50 \text{ m}$ and a UAV height up to $h_r = 30 \text{ m}$.

- (3) The use of the developed NLOS communication system at a wavelength of $\lambda = 510$ nm by the ground–UAV scheme allowed a stable communication to be organized at UAV heights up to $h_r = 45$ m and baseline distances up to 100 m. At baseline distances of $150 \leq Y_N \leq 385$ m, the NLOS communication was stable at $h_r \leq 20$ m. The maximum baseline distance of stable communication for this transceiver system was $Y_N \sim 385$ m.

The results obtained showed that, with the developed transceiver system, it is feasible to organize a stable NLOS optical communication channel between the ground points with relay via the UAV over a baseline distance of up to 510 m (385 m for the ground–UAV scheme at $\lambda = 510$ nm and 125 m by the UAV–ground scheme at $\lambda = 450$ nm). To improve the communication stability during a session and to communicate with a moving UAV, it is necessary to place the UAV-borne equipment on a rotating device that compensates for wind-driven deviations. In addition, it is necessary to automatically point the UAV-borne system at the coordinates of the ground position of the receiving (or transmission) system. This, in turn, increases the maximum range of stable NLOS communication with the UAV. The results obtained provide the basis for the design of NLOS communication systems with UAVs and can be used to test the capabilities of theoretical models of an NLOS communication channel.

Author Contributions: Conceptualization, M.V.T.; methodology, M.V.T., E.S.P. and A.V.F.; validation, E.S.P. and A.V.F.; formal analysis, E.S.P. and M.V.T.; investigation, E.S.P., A.V.F. and M.V.T.; writing—original draft preparation, M.V.T. All authors have read and agreed to the published version of the manuscript.

Funding: The study was carried out with the financial support of the Russian Science Foundation (Grant No. 22-22-00830).

Institutional Review Board Statement: Not applicable.

Informed Consent Statement: Not applicable.

Data Availability Statement: The data presented in this study are available on request from the corresponding author. The data are not publicly available due to the limitations of the Russian Science Foundation.

Conflicts of Interest: The authors declare no conflicts of interest.

References

1. Wang, C.X.; Huang, J.; Wang, H.; Gao, X.; You, X.; Hao, Y. 6G Wireless Channel Measurements and Models: Trends and Challenges. *IEEE Veh. Technol. Mag.* **2020**, *15*, 22–32. [[CrossRef](#)]
2. Ding, J.; Mei, H.; I, C.-L.; Zhang, H.; Liu, W. Frontier Progress of Unmanned Aerial Vehicles Optical Wireless Technologies. *Sensors* **2020**, *20*, 5476. [[CrossRef](#)] [[PubMed](#)]
3. Kong, H.; Lin, M.; Zhang, J.; Ouyang, J.; Zhu, W.P.; Alouini, M.-S. Beamforming Design and Performance Analysis for Satellite and UAV Integrated Networks in IoRT Applications. *IEEE Internet Things J.* **2022**, *9*, 14965–14977. [[CrossRef](#)]
4. Qu, L.; Xu, G.; Zeng, Z.; Zhang, N.; Zhang, Q. UAV-Assisted RF/FSO Relay System for Space-Air-Ground Integrated Network: A Performance Analysis. *IEEE Trans. Wirel. Commun.* **2022**, *21*, 6211–6225. [[CrossRef](#)]
5. Li, M.; Hong, Y.; Zeng, C.; Song, Y.; Zhang, X. Investigation on the UAV-To-Satellite Optical Communication Systems. *IEEE J. Sel. Areas Commun.* **2018**, *36*, 2128–2138. [[CrossRef](#)]
6. Mondal, A.; Hossain, A. Channel characterization and performance analysis of unmanned aerial vehicle-operated communication system with multihop radio frequency–free-space optical link in dynamic environment. *Int. J. Commun. Syst.* **2020**, *33*, e4568. [[CrossRef](#)]
7. Ajam, H.; Najafi, M.; Jamali, V.; Schober, R. Ergodic Sum Rate Analysis of UAV-Based Relay Networks With Mixed RF-FSO Channels. *IEEE Open J. Commun. Soc.* **2020**, *99*, 72–85. [[CrossRef](#)]
8. Agheli, P.; Beyranvand, H.; Emadi, M.J. UAV-Assisted Underwater Sensor Networks Using RF and Optical Wireless Links. *J. Light. Technol.* **2021**, *39*, 7070–7082. [[CrossRef](#)]
9. Singh, P.; Bohara, V.A.; Srivastava, A. On the Optimization of Integrated Terrestrial-Air-Underwater Architecture Using Optical Wireless Communication for Future 6G Network. *IEEE Photonics J.* **2022**, *14*, 7355712. [[CrossRef](#)]
10. Zhao, T.; Zhao, Y.; Liu, K. Wireless ultraviolet cooperative unmanned aerial vehicle formation communication link maintenance method. *Appl. Opt.* **2022**, *61*, 7140–7149. [[CrossRef](#)]

11. Singh, D.; Swaminathan, R. Comprehensive Performance Analysis of Hovering UAV-Based FSO Communication System. *IEEE Photonics J.* **2022**, *14*, 1–13. [[CrossRef](#)]
12. Ghanbari, M.; Ataee, M.; Sadough, S.M.S. Outage Performance Analysis for UAV-Based Mixed Underwater-FSO Communication Under Pointing Errors. In Proceedings of the 4th West Asian Symposium on Optical and Millimeter-Wave Wireless Communications (WASOWC), Tabriz, Iran, 12–13 May 2022; pp. 1–5. [[CrossRef](#)]
13. Park, S.; Yeo, C.I.; Heo, Y.S.; Ryu, J.H.; Kang, H.S.; Lee, D.-S.; Jang, J.-H. Tracking Efficiency Improvement According to Incident Beam Size in QPD-Based PAT System for Common Path-Based Full-Duplex FSO Terminals. *Sensors* **2022**, *22*, 7770. [[CrossRef](#)] [[PubMed](#)]
14. Dabiri, M.T.; Rezaee, M.; Mohammadi, L.; Javaherian, F.; Yazdani, V.; Hasna, M.O.; Uysal, M. Modulating Retroreflector Based Free Space Optical Link for UAV-to-Ground Communications. *IEEE Trans. Wirel. Commun.* **2022**, *21*, 8631–8645. [[CrossRef](#)]
15. Fawaz, W.; Abou-Rjeily, C.; Assi, C. UAV-Aided Cooperation for FSO Communication Systems. *IEEE Commun. Mag.* **2018**, *56*, 70–75. [[CrossRef](#)]
16. Weisman, M.J.; Dagefu, F.T.; Moore, T.J.; Arslan, C.H.; Drost, R.J. Analysis of the low-probability-of-detection characteristics of ultraviolet communications. *Opt. Express* **2020**, *28*, 23640–23651. [[CrossRef](#)]
17. Becker, D.; Fiebig, U.-C.; Schalk, L. Wideband Channel Measurements and First Findings for Low Altitude Drone-to-Drone Links in an Urban Scenario. In Proceedings of the 14th European Conference on Antennas and Propagation (EuCAP), Copenhagen, Denmark, 15–20 March 2020; pp. 1–5. [[CrossRef](#)]
18. Zhao, T.; Yu, X.; Liu, P.; Liu, L. Ultraviolet anti-collision and localization algorithm in UAV formation network. *Optik* **2019**, *192*, 162919. [[CrossRef](#)]
19. Tadayoni, H.; Ardakani, M.H.; Heidarpour, A.R.; Uysal, M. Ultraviolet Communications for Unmanned Aerial Vehicle Networks. *IEEE Wirel. Commun. Lett.* **2022**, *11*, 178–182. [[CrossRef](#)]
20. Tadayoni, H.; Uysal, M. Ultraviolet Communications for Ground-to-Air Links. In Proceedings of the 27th Signal Processing and Communications Applications Conference (SIU), Sivas, Turkey, 24–26 April 2019; pp. 1–4. [[CrossRef](#)]
21. Zhao, T.; Xie, Y.; Xu, S.; Wang, J.; Wang, H. Flocking of UAV Formation with Wireless Ultraviolet Communication. *Wirel. Pers. Commun. Int. J.* **2020**, *114*, 2551–2568. [[CrossRef](#)]
22. Sunstein, D.E. A Scatter Communications Link at Ultraviolet Frequencies. Bachelor's Thesis, Department of Electrical Engineering, Massachusetts Institute of Technology, Cambridge, MA, USA, 1968. Available online: <http://hdl.handle.net/1721.1/13670> (accessed on 14 November 2023).
23. Harvey G.L. *A Survey of Ultraviolet Communication Systems*; Naval Research Laboratory Technical Report; Naval Research Laboratory: Washington, DC, USA, 1964.
24. Vavoulas, A.; Sandalidis, H.G.; Chatzidiamentis, N.D.; Xu, Z.; Karagiannidis, G.K. A Survey on Ultraviolet C-Band (UV-C) Communications. *IEEE Commun. Surv. Tutor.* **2019**, *21*, 2111–2133. [[CrossRef](#)]
25. Ding, H.; Chen, G.; Majumdar, A.K.; Sadler, B.M.; Xu, Z. Modeling of non-line-of-sight ultraviolet scattering channels for communication. *IEEE J. Sel. Areas Commun.* **2009**, *27*, 1535–1544. [[CrossRef](#)]
26. Drost, R.J.; Sadler, B.M. Survey of ultraviolet non-line-of-sight communications. *Semicond. Sci. Technol.* **2014**, *29*, 11. [[CrossRef](#)]
27. Elshimy, M.A.; Hranilovic, S. Non-line-of-sight single-scatter propagation model for noncoplanar geometries. *J. Opt. Soc. Am. A* **2011**, *28*, 420–428. [[CrossRef](#)] [[PubMed](#)]
28. Chen, G.; Xu, Z.; Ding, H.; Sadler, B.M. Path loss modeling and performance trade-off study for short-range non-line-of-sight ultraviolet communications. *Opt. Express* **2009**, *17*, 3929–3940. [[CrossRef](#)] [[PubMed](#)]
29. Xu, C.; Zhang, H. Packet error rate analysis of IM/DD systems for ultraviolet scattering communications. In Proceedings of the MILCOM 2015—2015 IEEE Military Communications Conference, Tampa, FL, USA, 26–28 October 2015; pp. 1188–1193.
30. Liao, L.; Li, Z.; Lang, T.; Chen, G. UV LED array based NLOS UV turbulence channel modeling and experimental verification. *Opt. Express* **2015**, *23*, 21825–21835. [[CrossRef](#)] [[PubMed](#)]
31. Tarasenkov, M.V.; Belov, V.V.; Poznakharev, E.S. Estimation of optimal wavelengths for atmospheric non-line-of-sight optical communication in the UV range of the spectrum in daytime and at night for baseline distances from 50 m to 50 km. *J. Opt. Soc. Am. A* **2022**, *39*, 177–188. [[CrossRef](#)] [[PubMed](#)]
32. Belov, V.V.; Juwiler, I.; Blaunstein, N.; Tarasenkov, M.V.; Poznakharev, E.S. NLOS Communication: Theory and Experiments in the Atmosphere and Underwater. *Atmosphere* **2020**, *11*, 1122. [[CrossRef](#)]
33. Abramochkin, V.N.; Belov, V.V.; Gridnev, Y.V.; Kudryavtsev, A.N.; Tarasenkov, M.V.; Fedosov, A.V. Optoelectronic communication in the atmosphere using diffuse laser radiation: Experiments in the field. *Light Eng.* **2017**, *25*, 41–49.
34. Belov, V.V.; Gridnev, Y.V.; Kudryavtsev, A.N.; Tarasenkov, M.V.; Fedosov, A.V. Optoelectronic UV Communication on Scattered Laser Radiation. *Atmos. Ocean. Opt.* **2018**, *31*, 698–701. [[CrossRef](#)]
35. Tarasenkov, M.V.; Belov, V.V.; Poznakharev, E.S. Statistical Simulation of Characteristics of an Optical Communication Channel Based on Scattered Radiation with an Unmanned Aerial Vehicle. *Atmos. Ocean. Opt.* **2022**, *35*, 8–16. [[CrossRef](#)]

36. Kneizys, F.X.; Robertson, D.C.; Abreu, L.W.; Acharya, P.; Anderson, G.P.; Rothman, L.S.; Chetwynd, J.H.; Selby, J.E.A.; Shettle, E.P.; Gallery, W.O.; et al. *The MODTRAN 2/3 Report and LOWTRAN 7 Model*; U.S. Air Force Geophysics Laboratory: Hanscom, MA, USA, 1996.
37. Reeves, A.D.; Torres, E.; Cerrillo-Marchan, S.; Carrasco, R.; Lang, T.; Chen, G. Modeling and experiment verification for non-line-of-sight ultraviolet overwater communication channel under shore-to-vessel conditions. In Proceedings of the SPIE 11133, Laser Communication and Propagation through the Atmosphere and Oceans VIII, San Diego, CA, USA, 11–15 August 2019; pp. 1–6. [[CrossRef](#)]

Disclaimer/Publisher’s Note: The statements, opinions and data contained in all publications are solely those of the individual author(s) and contributor(s) and not of MDPI and/or the editor(s). MDPI and/or the editor(s) disclaim responsibility for any injury to people or property resulting from any ideas, methods, instructions or products referred to in the content.